Research Article

Numerical Studies on Bow Waves in Intense Laser-Plasma Interaction

Li Ning [ID],[1] **Mu Jie** [ID],[2] **and Kong Fancun**[1]

[1]*Merchant Marine College, Shanghai Maritime University, Shanghai 201306, China*
[2]*Center for Ultimate Energy, Shanghai Tech University, Shanghai 201210, China*

Correspondence should be addressed to Mu Jie; mujie@shanghaitech.edu.cn

Laser-driven wakefield acceleration (LWFA) has attracted lots of attention in recent years. However, few writers have been able to make systematic research into the bow waves generated along with the wake waves. Research about the bow waves will help to improve the understanding about the motion of the electrons near the wake waves. In addition, the relativistic energetic electron density peaks have great potential in electron acceleration and reflecting flying mirrors. In this paper, the bow waves generated in laser-plasma interactions as well as the effects of different laser and plasma parameters are investigated. Multidimensional particle-in-cell simulations are made to present the wake waves and bow waves by showing the electron density and momentum distribution as well as the electric field along x and y directions. The evolution of the bow wave structure is investigated by measuring the open angle between the bow wave and the wake wave cavity. The angle as well as the peak electron density and transverse momentum is demonstrated with respect to different laser intensities, spot sizes, plasma densities, and preplasma lengths. The density peak emits high-order harmonics up to 150 orders and can be a new kind of "flying mirror" to generate higher order harmonics. The study on the bow waves is important for further investigation on the electron motion around the wake waves, generation of dense electron beams, generation of high-order harmonics, and other research and applications based on the bow waves.

1. Introduction

Bow wave is a common phenomenon that can be observed in fluid and gas. When a ship sails in the sea, in addition to the backward Kelvin wave, a specific wave will also be generated at the bow position, which determines the outer boundary of the wave it makes [1], and this is the bow wave. The bow wave not only consumes ship's energy but also damages coastal facilities and over-water buildings. Therefore, reducing the impact of the bow wave is an important goal of shipbuilding industry. In the air, when the aircraft breaks through the sound barrier, it will trigger a specific bow wave and the associated Prandtl–Glauert condensation cloud [2].

Bow waves are also found in space, such as the bow shock wave produced when the solar wind meets the Earth's magnetic field. At present, the largest observed head wave is observed by the Spitzer Space Telescope in galaxy collision [3]. As can be seen from the above examples, bow waves can lead to a large number of physical processes, such as the transverse transfer of momentum and matter and particle acceleration.

It is well known that the ultra-short laser pulse propagating in the low-density plasma can excite the wake waves [4, 5], which is very similar to the Kelvin wave generated by the ship sailing in the sea. In addition to the wake waves, the laser pulse can also excite the bow waves in the collisionless plasma. Like a ship's bow wave, the bow wave generated by a laser pulse also disperses the energy and momentum of the laser pulse to the sides. The concept of bow waves in laser plasma was first proposed by Esirkepov et al. [6] in 2008. It was revealed that transverse modulation of electron density caused by the bow wave can effectively increase the potential of wakefield. In recent years, a large number of researchers have paid attention to laser wakefield acceleration (LWA)

[7–11], but few of them have detailed analysis about bow waves. Further study of bow waves will help to further understand the crucial problems of wakefield acceleration, such as the motion of electrons in the wakefield and bow wave, as well as the high-order harmonics generated by them.

Research about the electron motion related to the wakefield is important not only to the LWA but also to the radiation produced by the ultra-fast electron beam and the electron "flying mirror" regime. Coherent ultra-short radiation source is an important tool to explore and control the microcosmic world [12, 13]. The electron beam accelerated by the wakefield can generate ultra-short pulses and high-order harmonics [14, 15]. Moreover, high-frequency pulses [16] and self-generated magnetic field can be generated by using ultra-fast electrons to reflect the probe light [17].

When a focused laser pulse propagates in under-dense plasma, if the spot size of the laser is smaller than the wavelength of the wakefield, the electrons expelled by the laser cannot be trapped by the wakefield. The electrons will move to the sides, forming the bow wave of the wakefield. So far, there are few studies on the bow waves in laser plasma. In this paper, the effects of laser and plasma parameters on the bow wave properties are studied in detail. The density of the electron layer at the junction of the wakefield and the bow wave is much higher than that at the bottom of the wakefield, and the longitudinal velocity is close to the speed of light. By using the ultra-dense energetic electron layer at the joining part of the bow wave and wake wave as a "flying mirror" to reflect laser pulse, we can obtain high-order harmonics with upshifted frequency [18]. In this paper, we investigated how the open angle, transverse momentum of the bow wave, and the peak density are influenced by the initial density of plasma, laser intensity, focal spot size, and preplasma length. It helps to further understand the formation of the wakefield and bow wave, the mechanism of high-order harmonic generation, and coherent Thomson scattering.

2. Simulation Parameters

Two-dimensional and three-dimensional numerical simulations of the interaction between laser and under-dense plasma were carried out by particle-in-cell (PIC) code EPOCH [19]. In 2D simulations: the size of simulation box is $100\lambda_0 \times 100\lambda_0$, and the mesh number is 1600×800, where $\lambda_0 = 1\mu m$ is the wavelength of incident laser in vacuum. The number of macroparticles is 5120000. The fully ionized plasma is located at $20\lambda_0 \leq x \leq 100\lambda_0$, and the density is $n_e = 1.2 \times 10^{18}\text{cm}^{-3} \times (1\mu m/\lambda)$. The initial intensity of the laser pulse is $I = (6 \times 10^{19}W/\text{cm}^2) \times [(1\mu m/\lambda_0)^2]$, corresponding to the dimensionless amplitude $a = eE_0/\omega m_e c = 6.62$, which propagates forward along the x-axis and is linearly polarized along the y-axis, the full width at half maximum of the transverse focal spot is $10\mu m$, and the FWHM of the pulse width is $35fs = 10.5T_0$. ω is the laser frequency, e and m_e denote the charge and mass of the electron, E_0 is the amplitude of the laser electric field, c is the speed of light in vacuum, and T_0 is the laser period. The ions are assumed as

stationary, that is, the mass ratio of ion to electron is $m_i/m_e \longrightarrow \infty$.

The wakefield and bow wave can be observed in a wide range of parameters. Parameters in the three-dimensional simulation are as follows: the size of the simulation box is $22\lambda_0 \times 30\lambda_0 \times 30\lambda_0$, and the mesh number is $660 \times 900 \times 900$. The number of macroparticles is 5.35×10^8. The fully ionized plasma is distributed in the whole simulation space with the density of $n_e = 5.7 \times 10^{18}\text{cm}^{-3} \times (1\mu m/\lambda)$. The initial intensity of the laser pulse is $I = (9 \times 10^{19}W/\text{cm}^2) \times [(1\mu m/\lambda_0)^2]$, corresponding to the dimensionless amplitude $a = eE_0/\omega m_e c = 8.1$, which propagates forward along the x-axis and is linearly polarized along the y-axis, the FWHM transverse focal spot is $6.7\mu m$, and the FWHM pulse duration is $16.65fs = 5T_0$.

3. Simulation Results and Analysis

When the laser pulse enters the plasma region, a strong wakefield will be excited. Under the ponderomotive force and electromagnetic force of the laser field, electrons will be expelled to all directions to form a bubble structure without electrons inside, as shown in the electron density distribution in Figure 1. The electric field not only pushes the electrons in the longitudinal direction but also pushes the electrons in the transverse direction, forming bow waves on both sides of the wakefield.

For the wakefield and bow wave, two-dimensional simulation is launched for further analysis. The electron density distribution is shown in Figures 2(a)–2(d). Figures 2(b) and 2(c) show the distribution of electron density along the dotted line $x = 63\mu m$ and $y = 14\mu m$ in Figure 2(a), respectively. The electron number density at the bow wave reaches $9 \times 10^{18}\text{cm}^{-3}$. The electron density of the bow wave increases gradually along the $+x$ direction and reaches the maximum at the joining part of the bow wave and the wakefield. At this time ($78T_0$), the peak electron number density is about $4 \times 10^{19}\text{cm}^{-3}$, which is much higher than the density at the bottom of the wakefield, reaching more than 30 times the initial electron density. The ultra-dense electron layer at the joining part of the bow wave and wake wave has a velocity close to the speed of light. It can be used as a creative "flying mirror" to reflect laser pulses. According to the coherent Doppler effect, the frequency of the reflected laser pulse will be upshifted by $4\gamma^2$, where $\gamma = 1/\sqrt{1 - v^2/c^2}$, v is the velocity of the electron layer, and c is the speed of light in vacuum [20–22]. As shown in Figures 2(e) and 2(f), the distribution area of longitudinal electric field E_x is much larger than that of wakefield cavity. Thus, the potential is not limited by the wake cavity size.

The longitudinal and transverse electron momentum is shown in Figure 3. Due to transverse wave breaking, the electrons move outwards transversely, increasing the potential in the wakefield. Therefore, wake breaking is mainly aroused by the self-generated electrostatic field in the wakefield caused by the tightly focused laser [23]. The bow wave is piled up by the electrons directly accelerated by the laser ponderomotive force. When the laser enters the plasma, the electrons move forward and at the same time
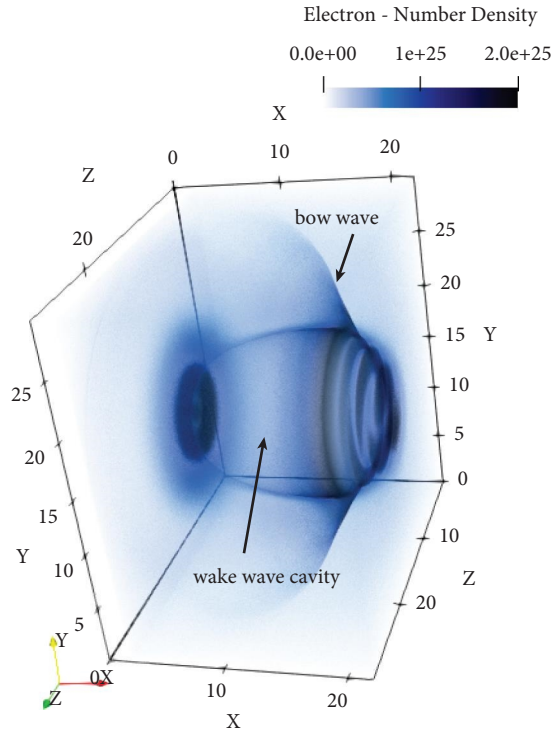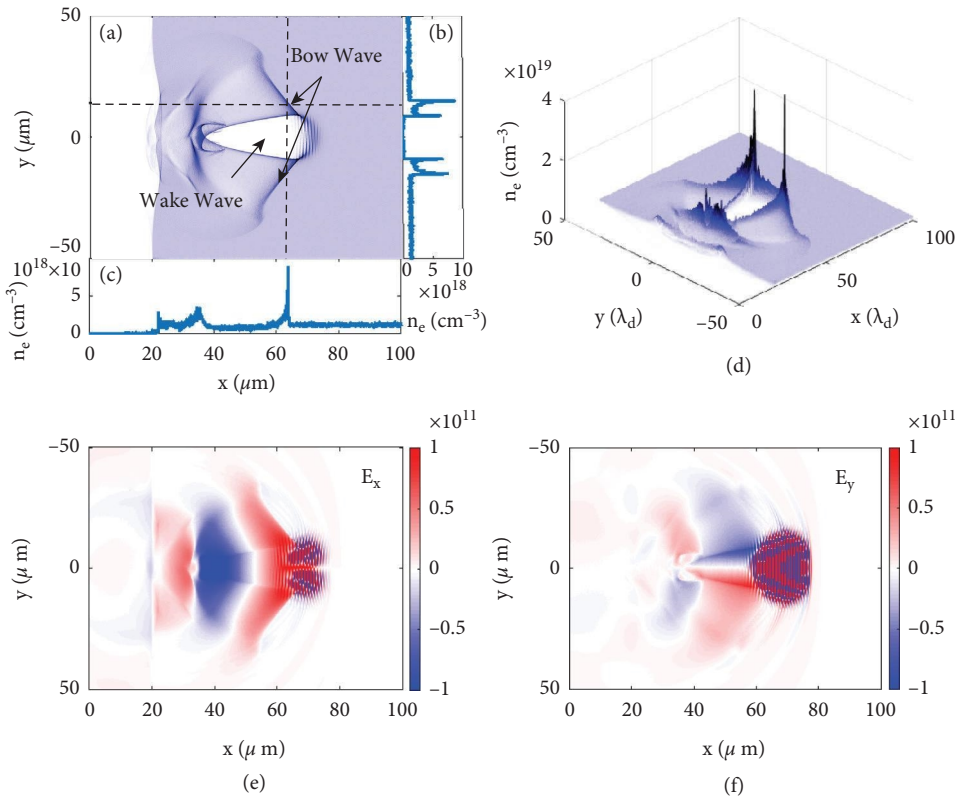
FIGURE 1: The electron density distribution at $24T_0$.

FIGURE 2: 2D simulation results at $78T_0$. (a)–(d) Electron density distribution in the (x, y) plane, (b) and (c) are the distributions along the dashed lines $x = 63\,\mu m$ and $y = 14\,\mu m$ in (a), (d) is the distribution with the number density shown in z-axis, and (e) and (f) are the longitudinal transverse electric fields, respectively, in the (x, y) plane.
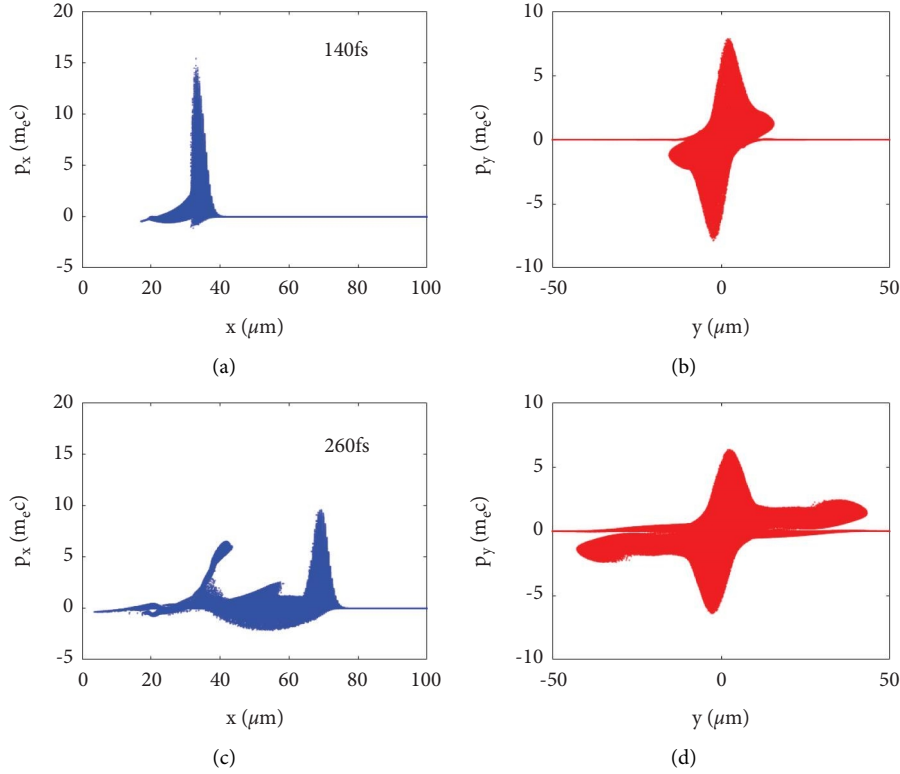
Figure 3: Longitudinal (a, c) and transverse (b, d) electron momentum at $42T_0$ and $78T_0$.

transversely to both sides continuously, gradually increasing the area of bow wave. Unlike the wake wave cavity easily being destroyed by electron injection, the properties of the bow wave are usually stable, as the laser propagates.

The structures of the wake waves and bow waves produced by different laser and plasma parameters are shown in Figure 4. The laser with higher intensity generates stronger ponderomotive force $F_p = -e^2/4m_e\omega^2\nabla E^2$. Therefore, with more intense laser, larger number of electrons will be expelled to the transverse sides, under larger ponderomotive force. As a result, the angle θ between the bow wave and the wake wave boundary is larger. The longitudinal length of the wake wave cavity is larger due to stronger electrostatic field and ponderomotive force, as shown in Figures 4(a) and 4(b). Denser plasma will repress the effect of ponderomotive force, resulting in shorter wake wave cavity and larger angle θ, as shown in Figures 4(c) and 4(d).

The laser focal spot size is $8\mu m$ and $20\mu m$, and the latter is closer to the matched spot size of a self-focused laser $w_0 = 2\sqrt{a_0}/k_p = 25\mu m$. Here $k_p = \sqrt{n_e e^2/m_e \varepsilon}/c$, where ε is the vacuum dielectric constant. The laser intensity hardly decays during the simulation with spot size of $20\mu m$ [24]. The electrostatic field is stronger and ponderomotive force is smaller, as shown in Figures 4(e) and 4(f). The preplasma can restrain the wave breaking and increase the energy of transverse ponderomotive force, so the distribution range of the bow wave in transverse direction is larger.

Laser and plasma parameters play important roles in the structure and distribution of wake wave and bow wave, as well as the electron momentum. The transverse momentum

distribution of electrons is shown in Figure 5. Increasing laser intensity will directly enhance the laser ponderomotive force and thus increase the transverse momentum of electron in wakefield and bow wave. Increasing electron density will lead to immature electron injection. The longitudinal momentum of the injected electron increases sharply, while the transverse and longitudinal momentum of the electron at the bow wave decreases. The focal spot size of the laser increases from $8\mu m$ to $20\mu m$, closer to the matched laser self-focusing radius. The laser with larger spot size makes the normalized electric field amplitude increase from $a_0 = 4.58$ to $a_0 = 6.58$, enhancing the wakefield and bow wave, as well as the electron momentum.

By changing the laser intensity, plasma density, laser focal spot size, and length of preplasma, the effects of laser and plasma parameters on the structure, density, and electron momentum of the bow wave are further studied. The bow wave can be produced within a wide range of parameters, but sometimes it is difficult to distinguish because it is located near the wake wave. It is found that the angle θ of the bow wave to the boundary of wake wave cavity is closely related to laser parameters such as laser intensity and focal spot radius. With higher laser intensity, θ increases obviously and the bow wave structure is easier to observe, as shown in Figures 4(a), 4(b), and 6(a). When the laser focal spot radius increases from $8\mu m$ to $20\mu m$, it is closer to the matched radius of the wakefield acceleration, and the wakefield energy and electron momentum are enhanced, but the angle θ between the bow wave and the wakefield wall decreases, as shown in Figures 4(e), 4(f), and 6(c). When the
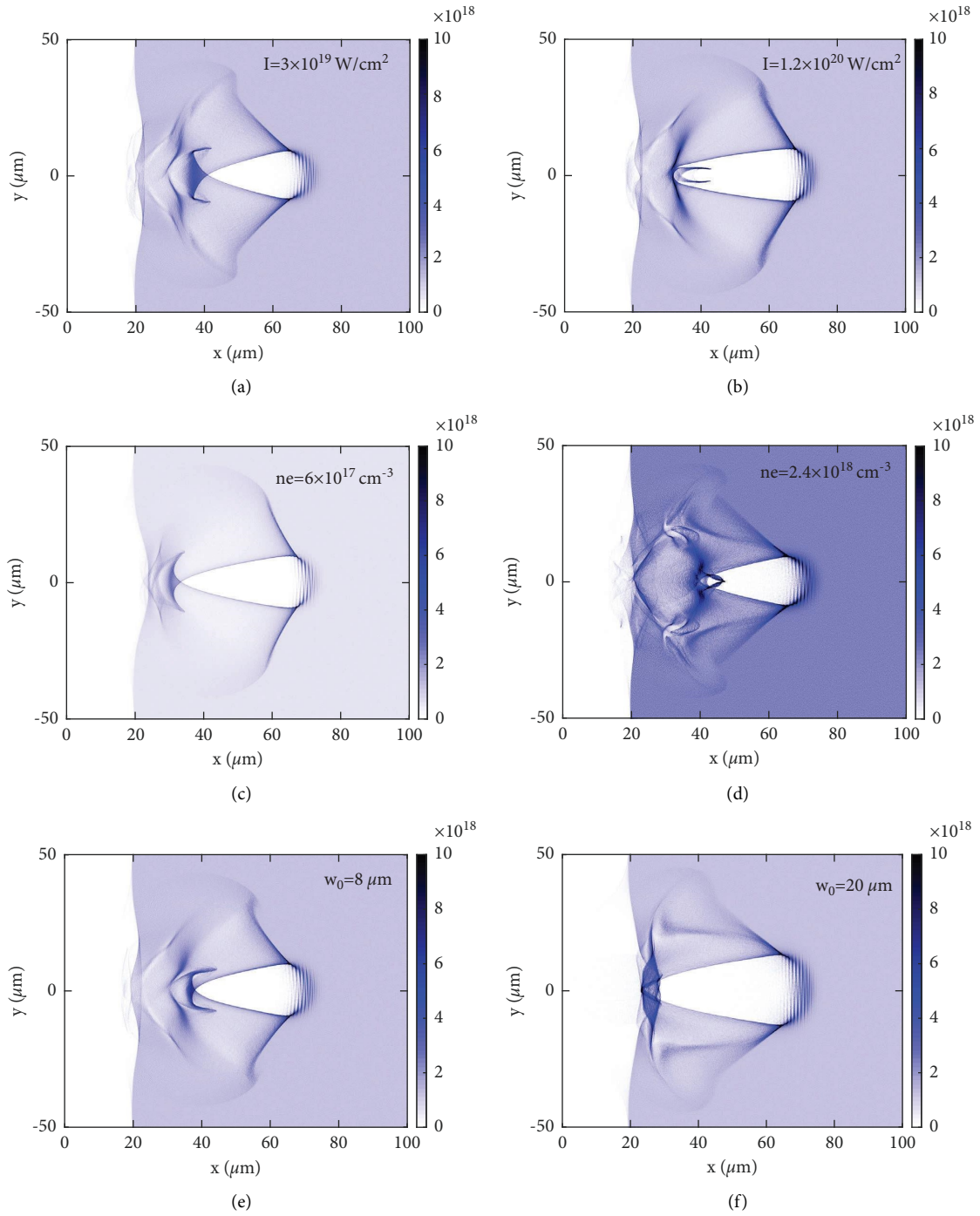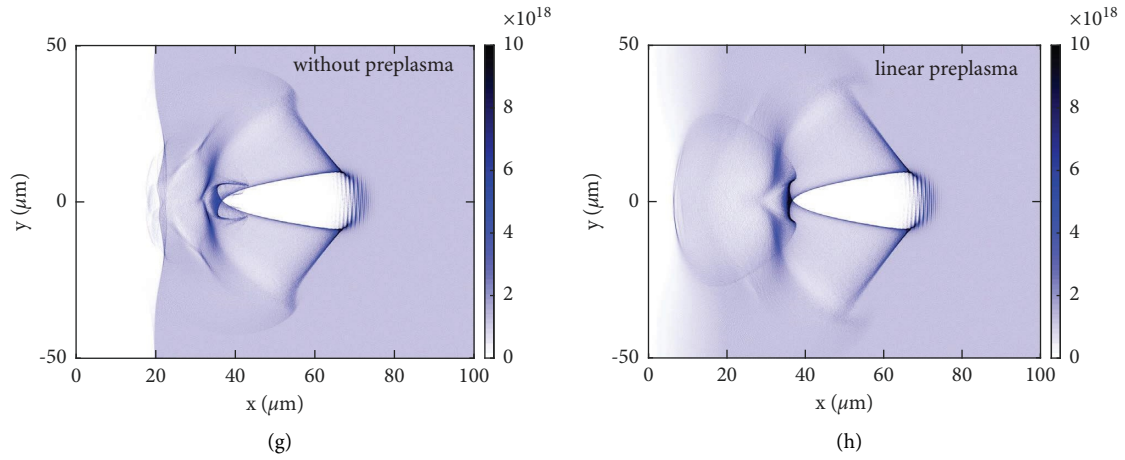
FIGURE 4: Continued.

(g)

(h)

FIGURE 4: Electron density distribution with respect to laser intensity of (a)$3 \times 10^{19} W/cm^2$ and (b)$1.2 \times 10^{20} W/cm^2$, plasma density of (c)$6 \times 10^{17} cm^{-3}$ and (d) $2.4 \times 10^{18} cm^{-3}$, and laser focal spot size of (e) 8μm and (f) 20μm (g) without preplasma and (h) with preplasma at $78T_0$.
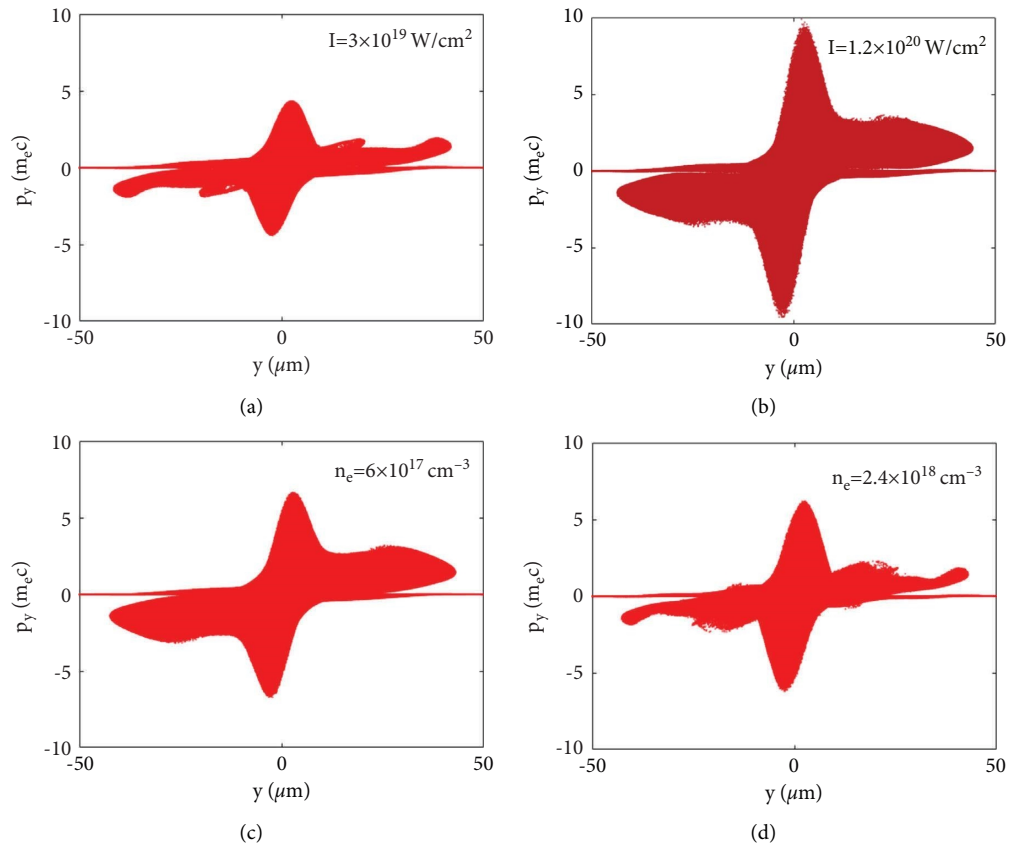

(a)

(b)

(c)

(d)

FIGURE 5: Continued.

(e)

(f)

(g)

(h)

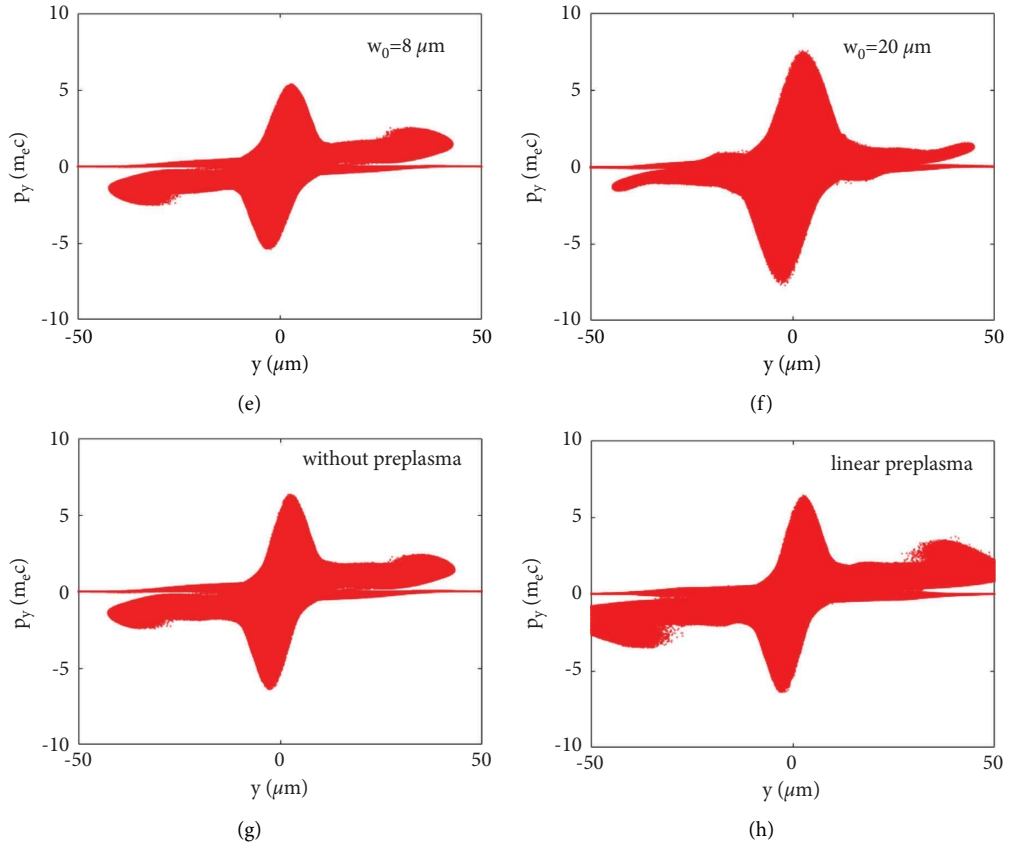FIGURE 5: Electron momentum distribution with respect to laser intensity of (a)$3 \times 10^{19} W/cm^2$ and (b)$1.2 \times 10^{20} W/cm^2$, plasma density of (c)$6 \times 10^{17} cm^{-3}$ and (d)$2.4 \times 10^{18} cm^{-3}$, and laser focal spot size of (e)$8\mu m$ and (f)$20\mu m$ (g) without consideration of preplasma and (h) linear increasing preplasma at $78T_0$.

--▽-- $I=3 \times 10^{19}$ W/cm^2
--○-- $I=6 \times 10^{19}$ W/cm^2
--△-- $I=1.2 \times 10^{20}$ W/cm^2

--▽-- $n_e=6 \times 10^{17}$ cm^{-3}
--○-- $n_e=1.2 \times 10^{18}$ cm^{-3}
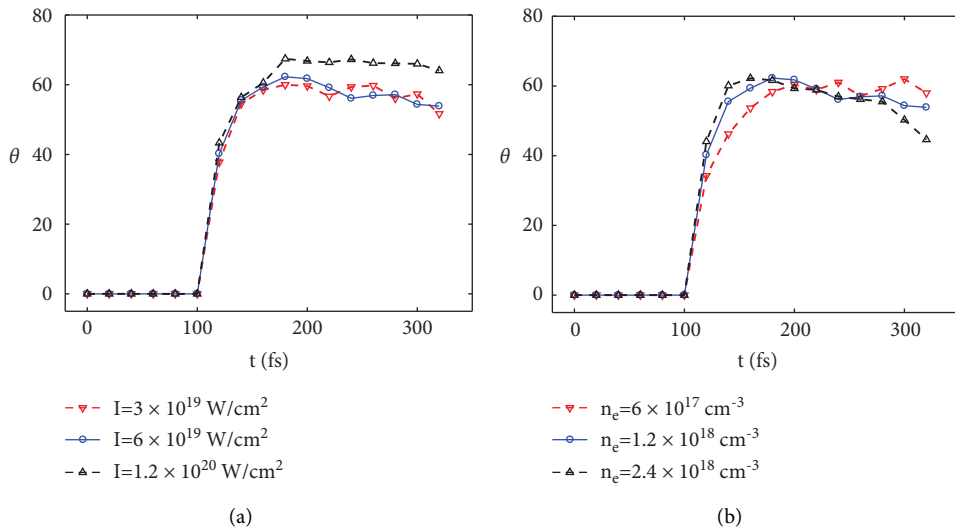--△-- $n_e=2.4 \times 10^{18}$ cm^{-3}
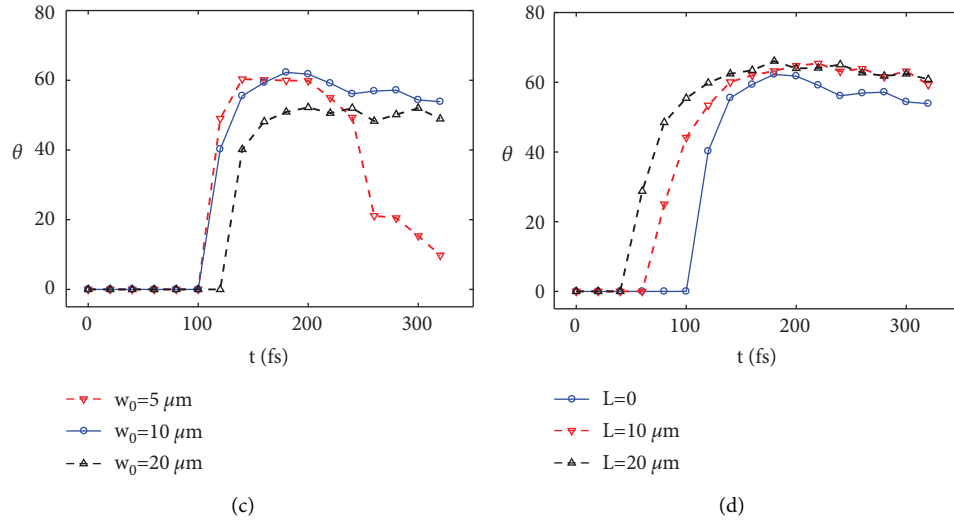
(a)

(b)

FIGURE 6: Continued.

(c)

(d)

FIGURE 6: The evolution of the angle between the wake wave cavity wall and the bow wave with respect to the laser and plasma parameters. (a)–(d) correspond to the influence of laser intensity, plasma density, laser spot size, and the length of preplasma.
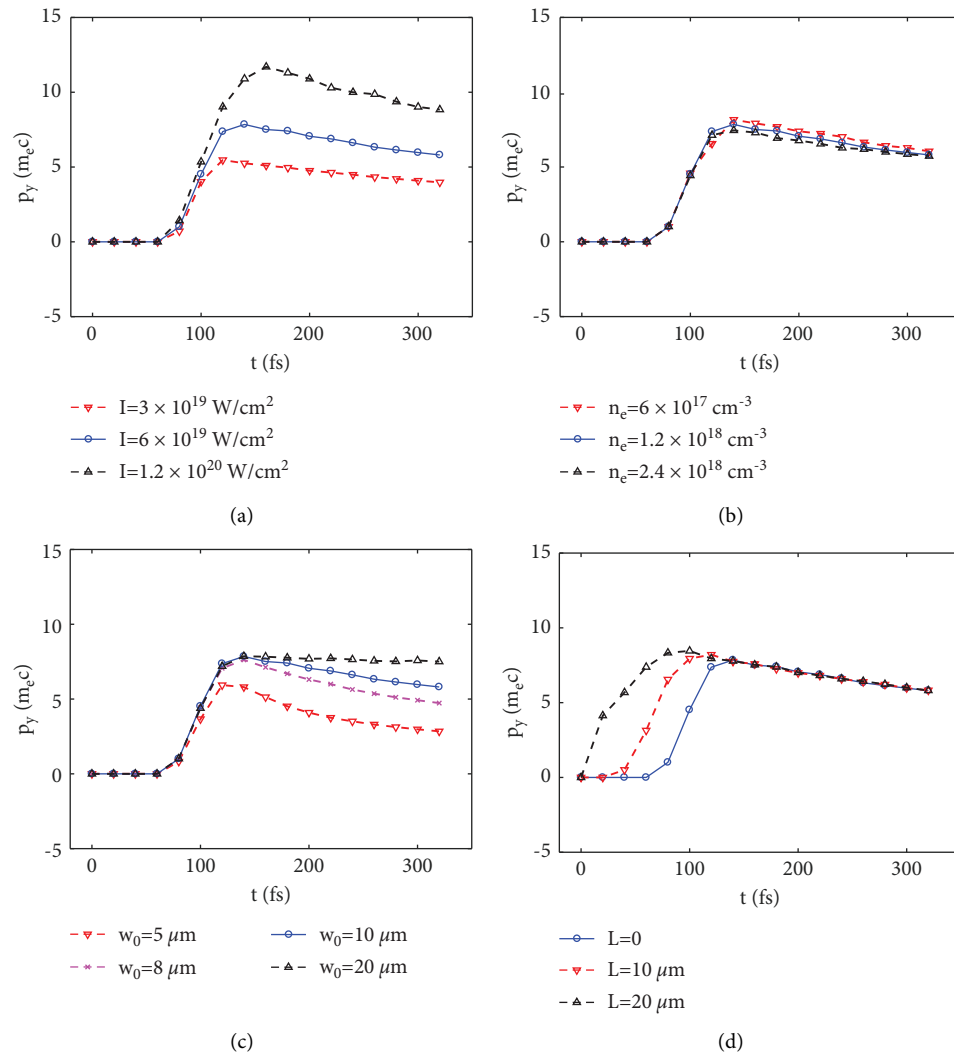

(a)

(b)

(c)

(d)

FIGURE 7: The evolution of the electron transverse momentum with respect to the laser and plasma parameters.
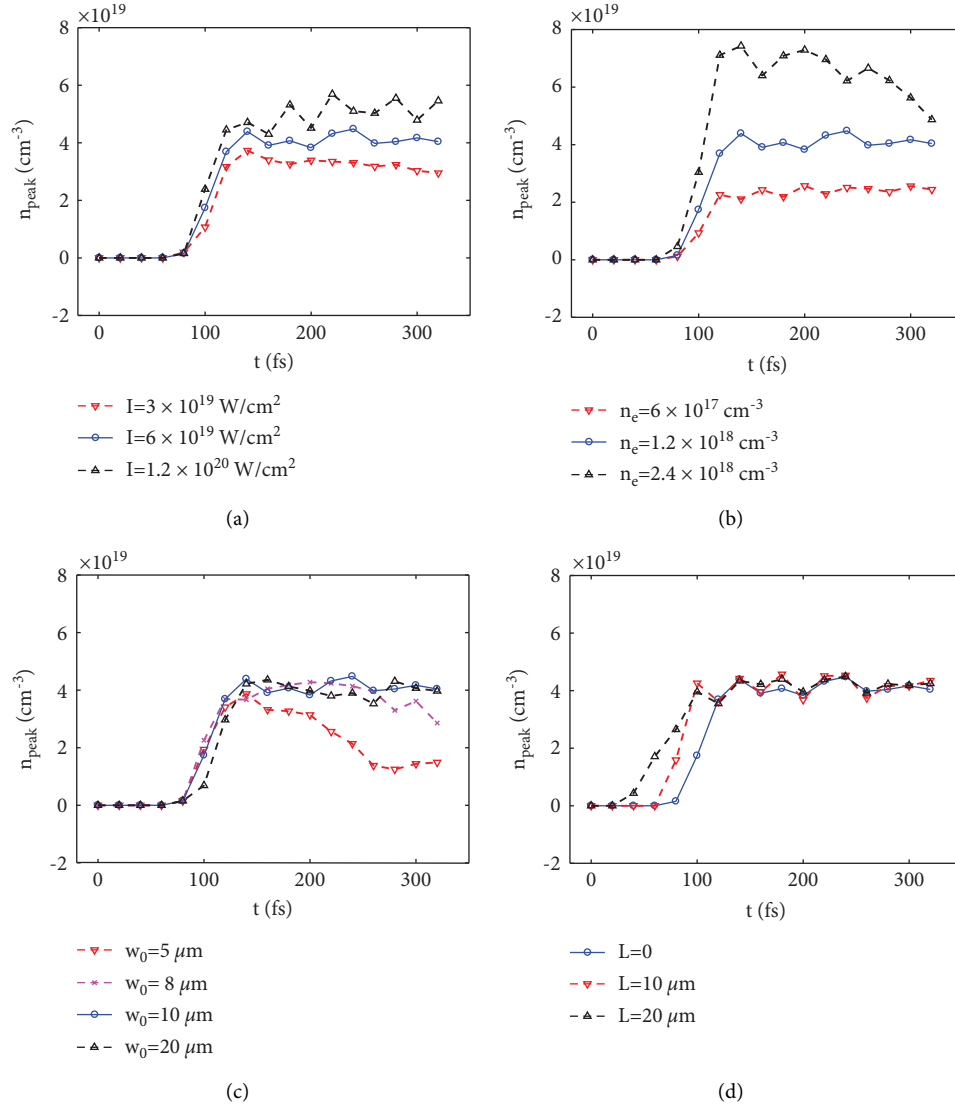
FIGURE 8: The evolution of the electron peak density of the bow wave with respect to the laser and plasma parameters.

laser focal spot is reduced to $5\mu m$, with the propagation of the laser, the laser will be defocused. With a_0 becoming smaller, θ decreases sharply and the shape of the bow wave becomes irregular. With increasing plasma density from $6 \times 10^{17} cm^{-3}$ to $2.4 \times 10^{18} cm^{-3}$, the angle θ decreases gradually, as shown in Figures 5(c), 5(d), and 6(b). When the pre-plasma is introduced, the angle θ is increased, as shown in Figures 5(g), 5(h), and 6(d).

As the laser interacts with the plasma, the electrons pile up to form the wake wave, and the electron transverse momentum increases. After the whole laser pulse entered the plasma and the wake wave cavity is completely formed, the transverse momentum of the electron decreases slowly, as shown in Figure 7. With the increase of laser intensity and focal spot radius, the transverse momentum of electrons increases significantly, enlarging the bow wave area. When the plasma density increases from $6 \times 10^{17} cm^{-3}$ to $2.4 \times 10^{18} cm^{-3}$, the transverse momentum and longitudinal momentum of electron decrease correspondingly until electron injection occurs. When the laser

focal spot increases, the transverse momentum of electron decreases more slowly. With a FWHM focal spot size of $w_0 = 20\mu m$, approximately equal to self-focusing matched size, the electron transverse momentum does not decay with time. The preplasma makes the laser interact with plasma earlier, and after the whole laser pulse entered the plasma, the electron transverse momentum is no longer influenced.

The electron density of the bow wave increases near the front and central area. A density peak is generated at the joining part of the bow wave and the wake cavity wall. The peak density fluctuates with time, but the overall trend is positively correlated with laser intensity and plasma density, as shown in Figures 8(a) and 8(b). This effect gets saturated when the laser intensity is over $1.2 \times 10^{20} W/cm^{-2}$ and when the density exceeds $2.4 \times 10^{18} cm^{-3}$. The peak density of the bow wave has no correlation with the size of the laser focal spot and the length of the preplasma, but when the laser focal spot is too small for the self-focusing effect, laser defocusing causes the density peak to decrease, as shown in Figures 8(c) and 8(d).

4. Conclusion

In this paper, multidimensional PIC code is used to simulate the generation of the wakefield and bow wave by the interaction of laser and plasma. By analyzing the influence of laser and plasma parameters on the structure of the bow wave, the peak electron density, and the electron momentum, the properties of the bow wave in the wakefield are further explored. The results show that increasing the laser intensity and reducing the plasma density are beneficial to the observation of the bow wave in the laser-induced wakefield, and the introduction of the preplasma is also helpful to observe the bow wave. When the focal spot size of the Gaussian laser beam is smaller than the matched self-focused laser in the wakefield, the transverse momentum of the electron is positively correlated with the focal spot radius. At the joining part of the bow wave and the wake cavity wall, the electron density is very high. The peak density is positively correlated with the laser intensity and plasma density. This high-density electron peak can be used as a new kind of electronic "flying mirror" to generate high-frequency high-order harmonics. This paper is innovative and forward-looking in the study of the bow wave of the wakefield, which is helpful to further understand the motion of electrons in the laser wakefield and bow wave, and has significance for the generation of high-frequency ultra-short pulses through a new kind of electronic "flying mirror." The work on laser and plasma is also beneficial to satellite laser communication.

Data Availability

The data used to support the findings of this study are included within the supplementary information file.

Conflicts of Interest

The authors declare that they have no conflicts of interest.

Acknowledgments

Supplementary Materials

The supplementary file includes the 2D density data of the simulation results. One can easily draw a 2D distribution of the density and see the bow waves. (*Supplementary Materials*)

References

[1] S. H. Lamb, *Hydrodynamics*, Cambridge Mathematical library, Cambridge, UK, 6th edition, 1993.

[2] T. Erich, *Fluidmechanik*, Springer, Berlin, Germany, 1996.

[3] P. N. Appleton, K. C. Xu, W. Reach et al., "Powerful high-velocity dispersion molecular hydrogen associated with an intergalactic shock wave in stephan's quintet," *The Astrophysical Journal*, vol. 639, no. 2, pp. L51–L54, 2006.

[4] T. Tajima and J. M. Dawson, "Laser electron accelerator," *Physical Review Letters*, vol. 43, no. 4, pp. 267–270, 1979.

[5] G. B. Zhang, Y. Y. Ma, D. B. Zou et al., "Effects of pulse transverse profile on electron bow-wave injection of electrons in laser wakefield acceleration," *Acta Physics of Sintering*, vol. 62, Article ID 125205, 2013, in Chinese.

[6] T. Z. Esirkepov, Y. Kato, and S. V. Bulanov, "Bow wave from ultraintense electromagnetic pulses in plasmas," *Physical Review Letters*, vol. 101, no. 26, Article ID 265001, 2008.

[7] E. Esarey, C. B. Schroeder, and W. P. Leemans, "Physics of laser-driven plasma-based electron accelerators," *Reviews of Modern Physics*, vol. 81, no. 3, pp. 1229–1285, 2009.

[8] W. P. Leemans, A. J. Gonsalves, H. S. Mao et al., "Multi-GeV electron beams from capillary-discharge-guided subpetawatt laser pulses in the self-trapping regime," *Physical Review Letters*, vol. 113, no. 24, Article ID 245002, 2014.

[9] J. Faure, C. Rechatin, A. Norlin, A. Lifschitz, Y. Glinec, and V. Malka, "Controlled injection and acceleration of electrons in plasma wakefields by colliding laser pulses," *Nature*, vol. 444, no. 7120, pp. 737–739, 2006.

[10] M. Litos, E. Adli, W. An et al., "High-efficiency acceleration of an electron beam in a plasma wakefield accelerator," *Nature*, vol. 515, no. 7525, pp. 92–95, 2014.

[11] G. H. Wang, X. F. Wang, and K. G. Dong, "Ultra-short ultra intense laser guiding and its influence on electron acceleration," *Acta Physica Sinica*, vol. 61, no. 16, Article ID 165201, 2012.

[12] F. Krausz and M. Ivanov, "Attosecond physics," *Reviews of Modern Physics*, vol. 81, no. 1, pp. 163–234, 2009.

[13] S. Corde, K. Ta Phuoc, G. Lambert et al., "Femtosecond x rays from laser-plasma accelerators," *Reviews of Modern Physics*, vol. 85, pp. 1–48, 2013.

[14] Z. M. Sheng, K. Mima, J. Zhang, and H. Sanuki, "Emission of electromagnetic pulses from laser wakefields through linear mode conversion," *Physical Review Letters*, vol. 94, no. 9, Article ID 095003, 2005.

[15] A. S. Pirozhkov, M. Kando, T. Z. Esirkepov et al., "Soft-X-ray harmonic comb from relativistic electron spikes," *Physical Review Letters*, vol. 108, no. 13, Article ID 135004, 2012.

[16] T. Z. Esirkepov, J. Mu, Y. Gu et al., "Optical probing of relativistic plasma singularities," *Physics of Plasmas*, vol. 27, no. 5, Article ID 052103, 2020.

[17] J. Mu, F. Y. Li, Z. M. Sheng, and J. Zhang, "Effect of transverse magnetic fields on high-harmonic generation in intense laser–solid interaction," *Laser and Particle Beams*, vol. 34, no. 3, pp. 545–551, 2016.

[18] J. Mu, T. Z. Esirkepov, P. Valenta et al., "High-order harmonics from laser irradiated electron density singularity formed at the bow wave in the laser plasma," *Physics of Wave Phenomena*, vol. 27, no. 4, pp. 247–256, 2019.

[19] T. D. Arber, K. Bennett, C. S. Brady et al., "Contemporary particle-in-cell approach to laser-plasma modelling," *Plasma Physics and Controlled Fusion*, vol. 57, no. 11, Article ID 113001, 2015.

[20] S. V. Bulanov, T. Z. Esirkepov, M. Kando, A. S. Pirozhkov, and N. N. Rosanov, "Relativistic mirrors in plasmas. Novel results and perspectives," *Physics-Uspekhi*, vol. 56, no. 5, pp. 429–464, 2013.

[21] M. Kando, A. S. Pirozhkov, K. Kawase et al., "Enhancement of photon number reflected by the relativistic flying mirror,"

Physical Review Letters, vol. 103, no. 23, Article ID 235003, 2009.

[22] J. Mu, F. Y. Li, M. Zeng, M. Chen, Z. M. Sheng, and J. Zhang, "Robust relativistic electron mirrors in laser wakefields for enhanced Thomson backscattering," *Applied Physics Letters*, vol. 103, no. 26, Article ID 261114, 2013.

[23] S. V. Bulanov, F. Pegoraro, A. M. Pukhov, and A. S. Sakharov, "Transverse-wake wave breaking," *Physical Review Letters*, vol. 78, no. 22, pp. 4205–4208, 1997.

[24] W. Lu, M. Tzoufras, C. Joshi et al., "Generating multi-GeV electron bunches using single stage laser wakefield acceleration in a 3D nonlinear regime," *Physical Review Special Topics-Accelerators and Beams*, vol. 10, no. 6, Article ID 061301, 2007.